Theoretical analysis of quantum transport, reflection and evaporation for helium-4 and application for dark matter detection.

Study of polarons and bipolarons in Bose-Einstein condensates.

Greis Cruz
Department of Physics, University at Buffalo
Buffalo, New York, USA.

under supervision of

Robert E. Zillich
Johannes Kepler University Linz
Linz, Austria

and

Eckhard Krotscheck
Department of Physics, University at Buffalo
Buffalo, New York, USA.

Contents

1 2-body problem with square well potential:

1.1 Behavior of the scattering length a

Calculate s-wave scattering length analytically and demonstrate that a diverges when you get a new bound state by increasing well depth V_0 or width r_c:

Considering the problem as a spherically symmetric problem, we have to solve the Schrödinger equation in spherical coordinates representation:

$$\left(\frac{-1}{2m}\nabla^2 + V(r) - E\right)\psi(r,\theta,\phi) = 0, \tag{1}$$

substituting the ansatz $\psi(r,\theta,\phi) = R_l(r)Y_{lm}(\theta,\phi)$ in the equation 1:

$$\left(\frac{1}{r^2}\partial_r(r^2\partial_r) - \frac{l(l+1)}{r^2} + 2m(E - V(r))\right)R_l(r) = 0, \tag{2}$$

where we have used the fact that the solution for the angular part include the eigenvalues $-l(l+1)$. With the usual substitution of the ansatz $R(r) = \chi/r$, it is obtained a more convenient representation of the Schrödinger equation:

$$\left(\partial_r^2 + 2m\left(E - V(r) - \frac{l(l+1)}{2mr^2}\right)\right)\chi_l(r) = 0 \tag{3}$$

The combination of the terms $V(r) + \frac{l(l+1)}{2mr^2}$ are called the "effective potential". The square well potential $V(r)$ can be mathematically represented as $V(r) = -V_0\Theta(R-r)$, being $\Theta(R-r)$ the Heaviside step function is illustrated in the figure 1, with R the extension of the well.

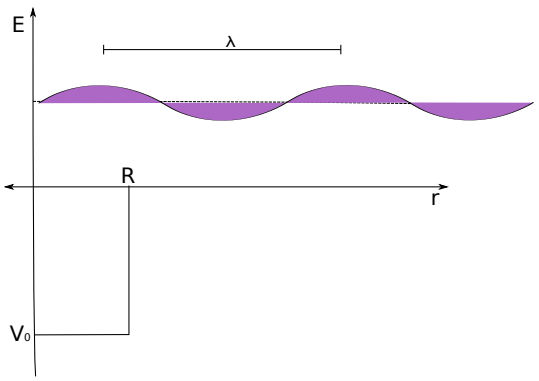

Figure 1: Well Potential in Spherical Coordinates

We are interested in the s-wave scattering length ($l = 0$), so the equation is simplified as:

$$\left(\partial_r^2 + 2m\left(E + V_0\Theta(R-r)\right)\right)\chi_l(r) = 0, \tag{4}$$

this equation has the general solution for $r > R$:

$$\chi(r) = \frac{i}{(2\pi)^{3/2}2k}(e^{-ikr} - \eta_0 e^{ikr}) = \frac{e^{i\delta_0}}{(2\pi)^{3/2}k}\sin(kr + \delta_0), \tag{5}$$

and for $r < R$,

$$\chi(r) = a_0 \sin(k_0 r). \tag{6}$$

As usual, we need to supply the requirement of the continuity of the wave function and its derivative at $r = R$.

$$\begin{aligned} \frac{e^{i\delta_0}}{(2\pi)^{3/2}k}\sin(kR + \delta_0) &= a_0 \sin(k_0 R) \\ \frac{e^{i\delta_0}}{(2\pi)^{3/2}k}\cos(kR + \delta_0) &= a_0 \cos(k_0 R). \end{aligned} \tag{7}$$

After doing the division between these two equations, the result is:

$$\delta_0 = \arctan\left(\frac{k}{k_i}\tan(k_0 R)\right) - kR. \tag{8}$$

Now, in the limit of vanishing energies, such a way that E is close to zero, the Schrödinger equation will looks like :

$$(\partial_r^2 + 2mE)\chi_l = 0, \tag{9}$$

so definitely the solution will be of the form:

$$\chi(r) = c_0(r - a), \tag{10}$$

where c_0 and a are constants. Also, we can get this result doing the expansion for small k in the sin function of the equation 5:

$$\chi(r) = c_1\left(r + \frac{\delta_0}{k}\right) + \mathcal{O}(k), \tag{11}$$

so, comparing the equations 10 and 11 we notice that for very small k, the $\mathcal{O}(k)$ will be negligible and the constant a will be defined as:

$$a = -\lim_{k\to 0}\frac{\delta_0}{k}, \tag{12}$$

The length scale a is the scattering length, and in the limit of very low energies ($E \approx 0$) , the target scatters as if it were a scattering area of $4\pi a^2$. a also sets the length scale when the wave function vanishes (different to the point in $r = 0$). In addition a has an important aspect because this quantity can assume infinitely large, positive or negative values; for studying these aspects we return to the result in the equation 12 but using the result of the well potential in the equation 8 [1]:

$$\begin{aligned} a &= -\lim_{k\to 0}\frac{1}{k}\left(\arctan\left(\frac{k}{k_0}\tan(k_0R)\right) - kR\right) \\ &\approx -\lim_{k\to 0}\frac{1}{k}\left(\frac{k}{k_0}\tan(k_0R) - \frac{1}{3}\left(\frac{k}{k_0}\tan(k_0R)\right)^3 ... - kR\right) \\ &= -\frac{\tan(k_0R)}{k_0} + R, \end{aligned} \tag{13}$$

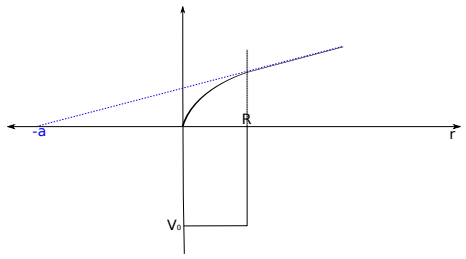

Figure 2: Negative scattering length

As we see, if $k_0R \approx \pi/2$, the scattering length becomes infinity, where k_0 is directly related with V_0 $\left(k_0 = \sqrt{2m(-V_0)}\right)$. Initially we can consider that $k_0R < \pi/2$ but not that small. So the solution in the potential region, takes the increasing part of the function $\sin(k_0R)$ and it has to match with the external function in an increasing slope, as it is shown in the figure 2. Doing the extrapolation of the linear solution we can see the intersection with the horizontal axis, this is the origin of the negative scattering length.

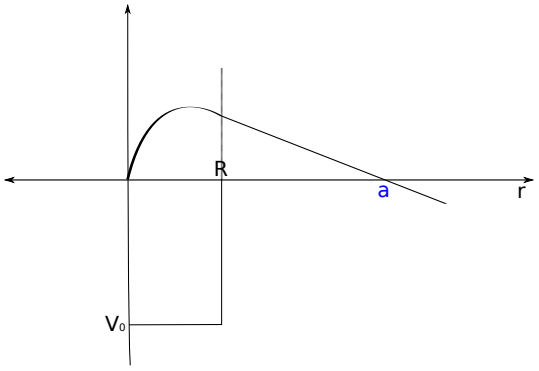

Figure 3: Positive scattering length

When we get more closer to $\pi/2$, the scattering length will take more negative values until $-\infty$, where a divergence occurs. Then we will get positive scattering length as you can see in the figure 3. This behavior is repeated again each π/R times. The general behavior of a versus k_0 is shown in the figure 4, where a sequences of divergences in $+\infty$ and $-\infty$ are displayed.

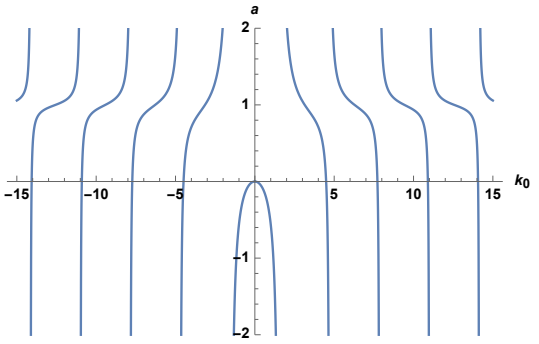

Figure 4: Behavior of the scattering length a vs k_0, when $R = 1$

Although the mathematical explanation is given, the physical point of view is more interesting because we can show the existence of bound states. Bound states are wave functions of finite spatial support and discrete spectrum, each divergence indicates a new bound state. Then, when k_0 (which depends on V_0) increases and a is positive we can get a bound state. The k_0 axis is going to be divided in ranges that goes from $\left(\frac{\pi}{2R} + \frac{n\pi}{R} < k_0 < \frac{\pi}{2R} + \frac{n\pi}{R} + \frac{(n+1)\pi}{R}\right)$ for n integer. In that way, the first range belongs to the first bound state, the second to a second bound state and so on. In summary: a singularity $a \to -\infty$ of the scattering length indicates

the scattering wave states and a singularity $a \to \infty$ of the scattering length signals the appearance of a zero energy bound state.

2 Quasiparticles (polarons)

The basic problem of a particle or an impurity moving and interacting with the environment has given the quantum explanation of several many body problems. Usually the Fröhlich Hamiltonian describes the motion of the impurity which is coupled with a boson system. The classical picture assumes that the bosons are phonons in a polar solid. This particle exert force upon the ions, which respond and move. The quantum nature of the phonons makes these forces occur in discrete units, and the ions motion, in the classical or quantum picture, in imaging as a polarization of the material around the particle. Of course the polarization affects the motion and energy of the particle [2].

3 HNC and Euler Equation

In the last decades, the confinement of ultra-cold systems have opened the research of new phenomena of theoretical interest. In that way, the interaction between the particles has an important influence on the quantum effects of the system. The interactions in turn depend on several parameters as the density, the potential strength or the scattering length. In this report I will introduce the study of an impurity in a bose system applying the hypernetted-chain Euler Lagrange method for the calculations of the ground state energy and correlation functions. This method has been used in the explanation of systems with two-body correlations and strong interactions[3]. We will present the basic theory [3, 4] of the HNC and the principal equations implemented in the code.

3.1 Bulk Liquid

3.1.1 Wave function

As usual, when the interactions between the particles become stronger, perturbation theory is no more applicable, we have to look for a different and more efficient method. Hence, we will us a variational approach that is able to describe the ground state until with three-body correlation functions and with the symmetry following the statistics of the bosons. Initially the Hamiltonian for a

strongly-interacting quantum many-body system is:

$$H = -\frac{\hbar^2}{2m}\sum_{i=1}^{N}\vec{\nabla}_i^2 + \sum_{i<j} v(|\vec{r}_i - \vec{r}_j|) \tag{14}$$

The ground-state wave function for a system of N identical boson with coordinates $\vec{r}_1, ...\vec{r}_N$ is written as a variational ansatz of the Jastrow-Feenberg form:

$$\psi(\vec{r}_1, ...\vec{r}_N) = \exp\frac{1}{2}\left(\sum_{i<j} u_2(\vec{r}_i, \vec{r}_j) + \sum_{i<j<k} u_3(\vec{r}_i, \vec{r}_j) + ...\right) \tag{15}$$

This function is able to describe the interactions for different ranges, as we demand that this function has the following properties:

1. For small $r_i - r_j$ the wave function is reduced to an effective two-body wave function.

2. For large $r_i - r_j$ the particles i and j are no longer correlated.

The most important component of the variational wave function is the two-body function $u_2(\vec{r}_i, \vec{r}_j)$, which describes both the short and long range correlations between pairs of particles. For the low density systems under consideration here an important aspect of the variational theory is the optimization of the correlations. The correlation functions are determined by the minimization of the energy-expectation value:

$$\frac{\delta}{\delta u_n}\left[\frac{\langle\psi_0|H|\psi_0\rangle}{\langle\psi_0|\psi_0\rangle}\right] = 0, \qquad n = 2, 3. \tag{16}$$

3.1.2 HNC and Euler Equation

The additional information needed to solve these equations is the connection between the correlation functions and the physically observable distribution functions. This connection is provided by the hypernetted chain (HNC) equations [5]. These equations are derived diagrammatic analysis of the two-body distribution function $g(r)$ in terms of the two-body correlation function. The analysis leads to the HNC relationships

$$g(r) = \exp[u_2(r) + N(r) + E(r)], \tag{17}$$

where $E(r)$ represents an infinite series of "elementary" diagrams which can be expressed as multi-dimensional integrals involving $g(r)$. The sum of nodal diagrams $N(r)$, can be expressed in momentum space. Introducing the dimensionless Fourier transform:

$$\tilde{f}(k) = \rho \int d^d r f(r) e^{i\vec{k}.\vec{r}}, \tag{18}$$

where d denotes the dimensionality of the system, and the static structure function:

$$S(k) = 1 + \rho \int d^d r e^{i\vec{k}.\vec{r}} [g(r) - 1], \tag{19}$$

introducing the function $\tilde{N}(k)$ as:

$$\tilde{N}(k) = \frac{(S(k) - 1)^2}{S(k)} = \frac{\tilde{X}^2(k)}{1 - \tilde{X}(k)} \tag{20}$$

where $\tilde{X}(k)$ is called the "direct correlation function" or the "non-nodal function":

$$\tilde{X}(k) = S(k) - 1 - \tilde{N}(k). \tag{21}$$

The level of the HNC approximation is defined by the choice of $E(r)$; e.g. HNC/0 neglects the elementary diagrams altogether, note that triplet correlations can be implemented through a modification of the definition of "elementary diagrams". The combination of the HNC equations 17 and the Euler equations 16 are generally referred to as the hypernetted-chain Euler-Lagrange (HNC-EL) theory. The correlation energy can be written as :

$$E = E_r + E_k + E_e + E_3 \tag{22}$$

where

$$\frac{E_r}{N} = \frac{\rho}{2} \int d^d r \left[(g(r) - 1) v(r) + \frac{\hbar^2}{m} |\nabla \sqrt{g(r)}|^2 \right], \tag{23}$$

$$\frac{E_k}{N} = -\frac{1}{4} \int \frac{d^d k}{(2\pi)^d \rho} t(k) (S(k) - 1) \tilde{N}(k), \tag{24}$$

$$\frac{E_e}{N} = -\frac{1}{4} \int \frac{d^d k}{(2\pi)^d \rho} t(k) (S(k) - 1) \tilde{E}(k), \tag{25}$$

here, $t(k) = \frac{\hbar^2 k^2}{2m}$ and E_3 is the contribution from triplet correlations. This term can be expressed in terms of the three-body correlation function $u_3(\vec{r}_1, \vec{r}_2, \vec{r}_3)$ and

the three-body distribution function. In this study we omit E_e and E_3 because they do not bring a new physical message.

The Euler-Lagrange equation can be conveniently written in coordinate space for the radial distribution function as:

$$-\frac{\hbar^2}{m}\nabla^2\sqrt{g(r)} + [v(r) + w_{ind}(r)]\sqrt{g(r)}, \tag{26}$$

where the "induced interaction" is

$$\begin{aligned}\tilde{w}_{ind}(k) &= -t(k)[S(k)-1] - \frac{1}{2}t(k)\left[\frac{1}{S^2(k)} - 1\right] \\ &= -t(k)[S(k)-1] - \tilde{V}_{p-h}(k).\end{aligned} \tag{27}$$

The coordinate space formulation of the Euler equation 26 includes the boson Bethe - Goldstone equation, which sums the dominant diagrams in the strong-coupling limit. An alternative formulation of the Euler equation 26 can be given in momentum space in terms of the structure factor $S(k)$,

$$S(k) = \left[1 + \frac{2}{t(k)}\tilde{V}_{p-h}(k)\right]^{-1/2}. \tag{28}$$

This equation is formally identical to the boson RPA expression for the structure factor. The HNC-EL theory supplements the RPA with a microscopic theory of the particle-hole interaction

$$V_{p-h}(r) = g(r)v(r) + \frac{\hbar^2}{m}|\nabla\sqrt{g(r)}|^2 + [g(r)-1]w_{ind}(r) \tag{29}$$

Equations 27, 28 and 29 can be solve iteratively for g(r) and S(k); they follow directly by carrying out the variation of the energy, equations 23 and 24, with respect to the pair distribution function $g(r)$. Of course, since the HNC equations , equations 17-20 provide a unique relationship between the pair correlation function $u_2(r)$ and the pair distribution function $g(r)$, we can also think of the Euler-equation as a variation with respect to $g(r)$:

$$\frac{\delta E}{\delta g}(r) = 0 \tag{30}$$

This will be important in view of the connection between the optimization condition and density functional theory.

3.1.3 Connection to parquet diagram theory

The formula 28 is readily identified with a boson RPA expression for the density -density response function:

$$\chi^{RPA}(k,\omega) = \frac{\chi_0(k,\omega)}{1-\tilde{V}_{p-h}\chi_0(k,\omega)} = \frac{2t(k)}{\hbar^2\omega^2 - \epsilon^2(k) - i\eta}. \tag{31}$$

with the response function of the non-interacting boson system:

$$\chi_0(k,\omega) = \frac{2t(k)}{\hbar^2\omega^2 - t^2(k) - i\eta}. \tag{32}$$

Then, it is seen that the static structure function $S(k)$ obtained from the Euler equation is identical to the one coming from the RPA expression

$$S(k) = \int_0^\infty -\frac{d\hbar\omega}{\pi} F_m \chi^{RPA} = \left[1 + \frac{4m}{\hbar^2 k^2}\tilde{V}_{p-h}(k)\right]^{-1/2}, \tag{33}$$

where F_m denotes the atomic form factor. Thus, the only quantity that can not immediately be understood in terms of Feynman perturbation theory is the induced interaction. "local parquet theory" localizes this interaction as follows:

- Begin with the RPA expression 31 and 33. Define an effective local two-body interaction $V_{eff}(r)$ such that the 2-body approximation for $S(k)$ with that local two-body interaction is the same as the RPA expression:

$$\chi^{(2)}(k,\omega) = \chi_0(k,\omega) + \chi_0(k,\omega)\tilde{V}_{eff}(k)\chi_0(k,\omega)$$

$$S^{(2)} = -\int_0^\infty -\frac{d\hbar\omega}{\pi} F_m^{(2)}\chi^{(2)}(k,\omega) = 1 - \frac{V_{eff}(k)}{t(k)} \tag{34}$$

- Demand that $S^{(2)}(k) = S(k)$. This defines the static effective interaction

$$\tilde{V}_{eff}(k) = t(k)(S(k) - 1) \tag{35}$$

We can think of the static effective interaction as an approximation for the dynamic effective interaction

$$\tilde{V}_{eff}(k) = \frac{\tilde{V}_{p-h}(k)}{1 - \tilde{V}_{p-h}(k)\chi_0(k,\omega)} \tag{36}$$

$$\tilde{V}_{eff}(k) = \tilde{V}_{eff}(k,\bar{\omega}), \tag{37}$$

which gives

$$\hbar^2\bar{\omega}^2 = -\frac{t^2(k)}{1+2S(k)} \tag{38}$$

comparing this with the equation 27 shows that,

$$\tilde{V}_{eff}(k) = \tilde{V}_{eff}(k) + \tilde{\omega}_{ind}(k). \tag{39}$$

Since we must identify $\tilde{V}_{eff}(k)$ with the local approximation of the set of particle-hole irreducible diagrams, and $\tilde{V}_{eff}(k)$ as the local approximation of the set of all two body vertices, we must identify the induced interaction as a local approximation of the set of all particle-hole reducible diagrams.

- In principle, the Bethe Goldstone equation should look like

$$-\frac{\hbar^2}{m}\nabla^2\phi(r,\omega) + \Big[v(r) + \omega(r,\omega)\Big]\phi(r,\omega) = 0, \tag{40}$$

i.e. it is an energy dependent equation. If the particle - hole interaction can be approximated by a local interaction, then

$$w_{ind}(k,\omega) = \frac{\tilde{V}_{p-h}(k)\chi_0(k,\omega)\tilde{V}_{p-h}(k)}{1-\tilde{V}_{p-h}(k)\chi_0(k,\omega)} \tag{41}$$

The dictum of "local parquet theory" is the to replace $w_{ind}(k,\omega) \approx w_{ind}(k,\bar{\omega})$ such that the Bethe-Goldstone equation gives the same $S(k)$. The question the Green's function people will normally ask is that how justified these approximation are and suggest different ones that are basically justified that they are doable, but without clear physical motivation. The quantitative motivation why exactly there approximations are the best is given by the fact that one can also evaluate the energy with Monte Carlo methods.

3.1.4 Exact relationships

It is evident from equation 28 that the condition $V_{p-h}(0+) > 0$ is a condition for the existence of solutions of the Euler equation. In the phenomenological interpretation of the RPA one can identify

$$mc^2 = V_{p-h}(0+) \tag{42}$$

where c is the speed of sound. On the other hand, the hydrodynamic compressibility K_T is obtained by differentiating the chemical potential with respect to density

$$mc^2 = \frac{d}{dp}\rho^2 \frac{d}{d\rho}\frac{E}{N} \tag{43}$$

The diagrammatic analysis of the HNC-EL equation reveals, however, that the microscopic 42 definition and the hydrodynamic definition 43 are identical only in an exact theory. This calls for some phenomenological modifications.

3.1.5 Connection to density functional theory

The use of the pair-distribution function as a variational function is analogous to using the one-body density in density functional theory. In fact, following the line of arguments leading to the Kohn - Hohenberg theorem for the one -body density. two statements can be made:

1. The kinetic energy T depends only on $g(r)$ and not on $v(r)$ and
2. The total energy has a minimum equal to the ground state energy at the physical ground state distribution function, in other words the ground state distribution function can be obtained by the variational principle in the equation 30.

The proof parallels exactly the proof given by Levy for the original Kohn-Hohenberg theorem and does not need to be repeated here. There is, however, an important corollary: Following the above, the total energy can be written as

$$E = T + V \tag{44}$$

where

$$V = \frac{\rho}{2}\int d^3 r v(r) g(r), \tag{45}$$

is the potential energy and T the kinetic energy whose form is yet unspecified, but it is known that T is a functional of $g(r)$ and not of $v(r)$. Replacing in equation 45 $v(r)$ by $\lambda v(r)$ and differentiation with respect to λ gives

$$\frac{dE}{d\lambda} = \frac{\rho}{2}\int d^3 r v(r) g_\lambda(r) + \int d^3 \frac{\delta E}{\delta g_\lambda(r)}\frac{dg_\lambda(r)}{d\lambda} \tag{46}$$

the second term in equation 46 vanishes, and hence the result for the energy from the coupling constant integration

$$E = \frac{\rho}{2} \int_0^1 d\lambda \int d^3 r v(r) g_\lambda(r) \tag{47}$$

is the same as the energy functional. However, the above derivation also shows that equation 47 is true not only for the exact ground state, but also for any approximate energy functional , as long as the pair distribution function is obtained by minimizing this approximate energy functional. This holds, therefore, for the HNC energy functional.

3.2 Single Impurity

3.2.1 Wave Function

Generally, we label background systems coordinates with a super/sub-script B, and impurity coordinate with a super/sub-script I. The impurity carries the coordinate r_0. The fact that there is only one foreign particle makes it possible to use the "old" solution for the background wave function $\psi(r_1, ..., r_N)$ and multiply that function with the correlation functions between the impurity and background. Since we are dealing with low density systems there is, unlike in the helium liquids, no need for triplet correlations:

$$\psi^I(r_0, r_1, ..., r_N) = \exp \frac{1}{2} \left[\sum_{j=1}^{N} u^{IB}(r_0, r_j) \right] \psi_0(r_0, r_1, ..., r_N) \tag{48}$$

The one particle density for the impurity is defined by integrating over all the background coordinates in the wave function,

$$\rho^I(r_0) = \frac{1}{N_0} \int d^3 r_1 ... d^3 r_N |\psi^I(r_0, ..., r_N)|^2 = \frac{1}{\Omega}; \tag{49}$$

it is equal to one over the total volume, Ω, of the system, which includes the impurity particle. Similarly, to obtain the impurity-background two-particle density, one integrates over all the other except one background coordinate.

$$\rho^I(r_0, r_1) = \frac{N}{N_0} \int d^3 r_2 ... d^3 r_N |\psi^I(r_0, ..., r_N)|^2, \tag{50}$$

where N_0 is the normalization integral

$$N_0 = \int d^3 r_0 ... d^3 r_N |\psi^I(r_0, ..., r_N)|^2. \tag{51}$$

The radial distribution function between the impurity and background particles is defined by

$$\rho^{IB}(r_0, r_1) = \rho^I(r_0)\rho^B(r_1)g^{IB}(r_0, r_1) \tag{52}$$

Note that $\rho^B(r_1)$ in equation 52 is the pure background density:

$$\rho^B(r_1) = N\frac{\int d^3r_2...d^3r_N|\psi(r_1, ..., r_N)|^2}{\int d^3r_1...d^3r_N|\psi(r_1, ..., r_N)|^2} = \frac{N}{\Omega_B} \tag{53}$$

3.2.2 HNC and Euler Equation

The chemical potential of the polaron can be written as:

$$\begin{aligned}\mu^I_{HNC} = \int d^3r_0 d^3r_1 \rho^I\rho^B \Bigg[& g^{IB}(r_0, r_1)V^{IB}(|r_0 - r_1|) \\ & + \frac{\hbar^2}{2m_I}|\nabla_0\sqrt{g^{IB}(r_0, r_1)}|^2 + \frac{\hbar^2}{2m_B}|\nabla_1\sqrt{g^{IB}(r_0, r_1)}|^2\Bigg] \\ -\frac{1}{2}\int \frac{d^3k}{(2\pi)^3\rho^B}\frac{\hbar^2k^2}{4}[S^{IB}(k)]^2\frac{S^{BB}(K) - 1}{S^{BB}(k)}&\left(\frac{1}{m_I} + \frac{1}{m_B} + \frac{1}{m_B S^{BB}k}\right)\end{aligned} \tag{54}$$

The variation of the chemical potential with respect to the impurity-background distribution function is a straight forward exercise. We first calculate:

$$\begin{aligned}0 = \frac{1}{2}\frac{\delta\mu^I}{\delta\sqrt{g^{IB}(r_0, r_1)}} = -&\left(\frac{\hbar^2}{2m_I}\nabla_0^2 + \frac{\hbar^2}{2m_B}\nabla_1^2\right)\sqrt{g^{IB}(r_0, r_1)} \\ &+[V(|r_0 - r_1|) + w_I^{IB}(r_0, r_1)]\sqrt{g^{IB}(r_0, r_1)}\end{aligned} \tag{55}$$

The last term in equation 55, $w_I^{IB}(r_0, r_1)$, is the phonon induced interaction. This term originates from the last part of the HNC approximation 54 for the chemical potential. It is most conveniently written in momentum space as:

$$w_I^{IB} = \frac{-1}{2}\frac{S^{IB}(k)(S^{BB}(K) - 1)}{S^{BB}(K)}\left(t_I(k) + t_B(k) + \epsilon(k)\right) \tag{56}$$

where we denote the kinetic energies by

$$t_I(k) = \frac{\hbar^2}{2m_I}k^2, \qquad t_B(k) = \frac{\hbar^2}{2m_B}k^2 \tag{57}$$

and the background excitation mode in Feynman approximation by

$$\epsilon(k) = \frac{\hbar^2}{2m_B}\frac{k^2}{S^{BB}(k)} \tag{58}$$

The Euler equations are most conveniently solved iteratively in momentum space; a few manipulations are required for that purposes. We multiply the whole equation 55 with $\sqrt{g^{IB}(r_0 r_1)}$ and introduce the particle-hole interaction, which gives the direct interaction between particles:

$$V^{IB}_{p-h}(r_0, r_1) = g^{IB}(r_0, r_1)V(|r_0 - r_1|) + \frac{\hbar^2}{2m_I}|\nabla_0\sqrt{g^{IB}(r_0, r_1)}|^2 + \frac{\hbar^2}{2m_B}|\nabla_1\sqrt{g^{IB}(r_0, r_1)}|^2 + (g^{IB}(r_0, r_1) - 1)w^{IB}_I(r_0, r_1) \tag{59}$$

With this notation, the two-particle Euler equation in momentum space has the form:

$$S^{IB}(k) = -2\frac{V^{IB}_{p-h}(k)S^{BB}(k)}{t_I(k) + \epsilon(k)} \tag{60}$$

3.2.3 Connection to Parquet diagrams

The connection to parquet theory goes in exactly the same was as above: The RPA for the impurity - background response function is

$$\chi_{IB}(k, \omega) = \chi^{II}_0(k, \omega)\tilde{V}^{IB}_{p-h}(k)\chi^{BB}_0(k, \omega) = \frac{4t_I(k)V^{IB}_{p-h}(k)t_B(k)}{((\omega - i\eta)^2 - t^2_I(k))((\omega - i\eta)^2 - \epsilon^2(k))} \tag{61}$$

which gives 61 through

$$S^{IB}(k) = -\int_0^\infty \frac{d\omega}{\pi}F_m\chi_{IB}(k, \omega) \tag{62}$$

Now do the same as above

- Define a local effective interaction

$$\chi^{(2)}_{IB}(k, \omega) = -\chi^{II}_0(k, \omega)\tilde{V}^{IB}_{eff}(k)\chi^{II}_0(k, \omega) \tag{63}$$

giving

$$S^{(2)}_{IB}(k) = -\int_0^\infty \frac{d\hbar\omega}{\pi}F_m\chi^{(2)}_{IB}(k, \omega) = \frac{2V^{IB}_{eff}(k)}{t_I(k) + t_B(k)} \tag{64}$$

- Demand $S_{IB}^{(2)}(k) = S_{IB}(k)$. This gives

$$\tilde{V}_{eff}^{IB}(k) = \tilde{V}_{p-h}^{IB}(k) S^{BB}(k) \frac{t_B(k) + t_I(k)}{\epsilon(k) + t_I(k)} \tag{65}$$

  Note again that

$$\tilde{V}_{eff}^{IB}(k) = \tilde{V}_{p-h}^{IB}(k) + \tilde{\omega}_I^{IB(k)} \tag{66}$$

- We can again think of this as taking the energy dependent effective interaction

$$\tilde{V}_{eff}^{IB}(k,\omega) = \frac{\tilde{V}_{p-h}^{IB}(k)}{1 - \tilde{V}_{p-h}^{BB}(k)\chi_0^{BB}(k,\omega)} \tag{67}$$

  at an average frequency

$$\tilde{V}_{eff}^{IB}(k,\omega) = \tilde{V}_{eff}^{IB}(k,\bar{\omega}) \tag{68}$$

  which gives

$$\hbar^2\omega^2 = \frac{t_B(k) t_{I(k)} \epsilon(k)}{t_B(k) + t_I(k) + \epsilon(k)} \tag{69}$$

3.2.4 Exact relationships

Equation 49-53 determine the volume integral:

$$\int d^3 r_1 g^{IB}(r_0, r_1) = \Omega_B \tag{70}$$

The volume occupied by one ^4He particle, $v_B = \Omega_B/N$ is different from the volume $v_i = \Omega - \Omega_B$ occupied by the impurity particle. This difference has consequences for the sequential relation for the impurity radial distribution function of equation 52:

$$\int d^3 r_1 \rho^B(r_1)[g^{IB}(r_0, r_1) - 1] = -\frac{v_I}{v_B} = -\beta \tag{71}$$

Here we have introduced the volume excess factor β, which is an important experimental parameter. The impurity structure function is the Fourier transform of the radial distribution function

$$S^{IB}(k) = \rho^B \int d^3 r e^{i\vec{k}.\vec{r}} [g^{IB}(r) - 1] \tag{72}$$

and its value at the origin,

$$S^{IB}(0+) = -\beta \tag{73}$$

It is given by the sequential relation 71. In the definitions 49 and 53 we have already made the assumption that our system is homogeneous, which makes it possible to take the Fourier transform with respect to the relative coordinate alone. From now we shall ignore the coordinate argument in the density factors. The volume excess factor is a measurable quantity and when it is well determined, like for the ^3He impurity, it can be used to calculate the impurity chemical potential by integrating the equation

$$\beta = \rho^B(P) \frac{d\mu^I}{dP} \tag{74}$$

over the pressure. These two relations can be used as a check of consistency of the theory in a similar manner as the thermodynamic compressibility can be used as a check of consistency of the theory in a similar manner as the thermodynamic compressibility can be used to test the consistency of the slope of the structure function in the long wave length limit.

3.3 Impurity-Impurity Interaction

The wave function of two impurities, located at r_0 and r_0' is:

$$\psi^{II}(r_0, r_0'; r_1, ..., r_N) = \exp \frac{1}{2} \Big[u^{II}(r_0, r_0') + \sum_{j=1}^{N} [u^{IB}(r_0, r_j) + u^{IB}(r_0', r_j) + u^{IIB}(r_0, r_0', r_j)] + \frac{1}{2} \sum_{j,k=1, j\neq k}^{N} [u^{IBB}(r_0, r_j, r_k) + u^{IBB}(r_0', r_j, r_k)] \Big] \psi_0(r_1, ..., r_N). \tag{75}$$

The situation for the two impurity case differs from the above ones because the wave function 75 can only lead to an effective impurity-impurity potential determining the impurity-impurity correlation function $u^{II}(r_0, r_0')$. This is exactly the

quantity we want because it gives us the information on the configuration. Its form has, in HNC approximation, been first derived by Owen [6]; adding "elementary diagram" and "triplet correlation" corrections, the effective interaction is

$$V_{eff}(r) = V^{(II)}(r) + w_{ind}(r) + V_e(r), \tag{76}$$

where $V^{(II)}(r)$ is the bare interaction between the two impurities, $V_e(r)$ the correction from "elementary" diagrams and triplets, and $w_{ind}(r)$ is the induced originating from phonon exchange and higher-order processes. The induced potential can depend only on background and single-impurity quantities.

Jastrow-Feenberg theory provides a prescription for calculating the induced potential mediated by the density fluctuation background, i.e. phonon exchange [6]:

$$\tilde{w}_{ind}(r) = \tilde{V}_{ind}(k, \tilde{w}(k)) = -\frac{\hbar^2 k^2}{4m}\left[\frac{S_{IB}(k)}{S(k)}\right]^2\left[2\frac{m}{m_I}S(k) + 1\right] \tag{77}$$

One can interpret this term from linear response theory: The full interaction between two polarons is strictly speaking energy dependent, it is the sum of the induced and the bare interaction,

$$V_{eff}(r, w) = V_{II}(r) + V_{ind}(r, w) \tag{78}$$

where

$$\tilde{V}_{ind}(k, w) = \tilde{V}_{IB}(k)\chi(k, w)\tilde{V}_{IB}(k) + \tilde{V}_e(k) \tag{79}$$

and $\chi(k, w)$ is the density-density response function of background, V^{IB}_{p-h} is the particle-hole potential, and $\tilde{V}_e(k)$ consists of contributions from triplets and elementary diagrams. The HNC-EL result is obtained by taking the density-density response function at an average imaginary frequency that is chosen according to the localization rules of parquet-diagram theory.

If one looks at the phonon exchange of weakly bound polarons pairs, one might therefore argue that it is better to take $w = 0$ which leads to a slightly different effective interaction

$$\tilde{w}_{ind}(k) = \tilde{V}_{ind}(k, w = 0) = -\frac{\hbar^2 k^2}{4m}\left[\frac{S_{IB}(k)}{S(k)}\right]^2\left[\frac{m}{m_I}S(k) + 1\right] \tag{80}$$

We will see, however, that there is little difference between the predictions of these two procedures for calculation the induced interaction.

4 Lennard-Jones and Pöeschl-Teller Potential

4.1 Lennard-Jones Potential

At substantially low T, most inert gases form solids at ambient pressure, they crystalize in close-packed structures (CCP or HCP). What is the binding force that holds an inert gas crystal together? The general form of the potential is giving by:

$$\phi(r) = -\frac{A}{r^6} + \frac{B}{r^{12}} = 4\epsilon\left[\left(\frac{\sigma}{r}\right)^{12} - \left(\frac{\sigma}{r}\right)^{6}\right], \tag{81}$$

also known as the Van der Waals interaction. This interaction contains a weak attractive term and a strong short-range repulsive term. For understanding this terms we need to realized what is the "source" of the Lennard-Jones potential, due to that inert gas has no monopole or dipole potential (the charge distribution of inert gas atoms is spherical), also the electron wave function has a negligible and repulsive wave function overlap and the chemical hybridization is also negligible.

We can concentrate first on the dispersion force (the attractive term), this is due to the so called the London dispersion force. Although the overall electron density of an atom is spherical, there is always a fluctuating (instantaneous) dipole moment $\vec{p}_1$ on one atom 1 at any given time.

The fluctuating dipole generates an electric field on atom 2 located at position $\vec{r}$

$$\vec{E}(\vec{r}) = -\frac{3\hat{r}(\vec{p}_1.\hat{r}) - \vec{p}_1}{r^3} \tag{82}$$

This electric fiend induces a dipole moment $\vec{p}_2$ in atom 2 proportional to the field:

$$\vec{p}_2 = \alpha\vec{E} = \alpha\frac{3\hat{r}(\vec{p}_1.\hat{r}) - \vec{p}_1}{r^3} \tag{83}$$

where α is the polarizability of atom 2. The interaction energy between the two dipoles is then

$$\frac{\vec{p}_1.\vec{p}_2 - 3(\hat{r}.\vec{p}_1)(\hat{r}.\vec{p}_2)}{r^3} \tag{84}$$

since

$$\vec{p}_2 = \alpha\frac{3\hat{r}(\vec{p}_1.\hat{r}) - \vec{p}_1}{r^3} \approx -\frac{1}{r^6} \tag{85}$$

which allow us to get the dispersion term (r^{-6}).

In the another hand, the (repulsive) $1/r^{12}$ term come from the repulsion of electrons when their wave functions overlap, which is a consequence of the Pauli exclusion principle (it is not the only reason). In addition the exponent 12 is phenomenological. Other empirical forms for the repulsive potential are also used in literature. The two parameters, ϵ and σ, measure the strength of the attractive interaction and the radius of the repulsive core. Fig 5.

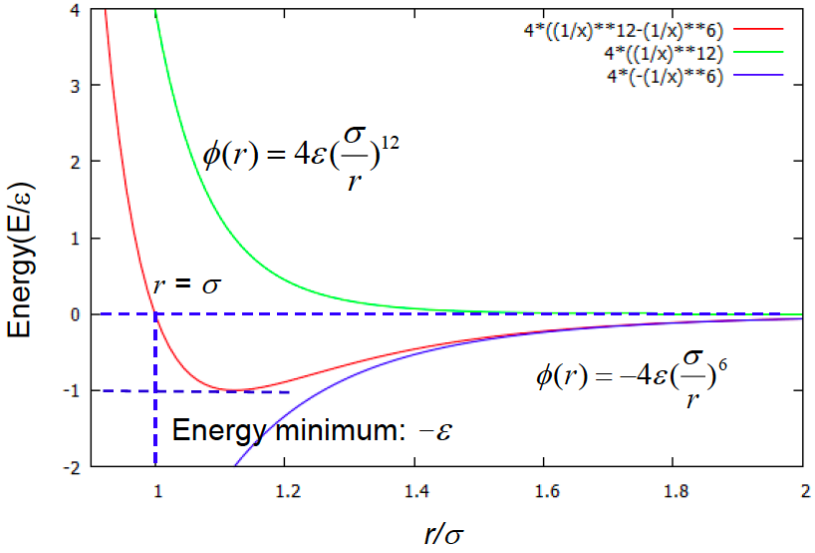

Figure 5: Lennard Jones Potential

4.1.1 Scattering Length for the Lennard Jones Potential

J. Pade in his work of 2007 [7], calculated the mathematical expression for the scattering length of a general modified Lennard-Jones interaction potential of the form or the equation 86:

$$V(r) = u\left[\left(\frac{r_0}{r}\right)^{2n-2} - \left(\frac{r_0}{r}\right)^{n}\right] \tag{86}$$

where the s-wave scattering length was presented. Due to nowadays it is suffice just use the scattering length for describing all the scattering dynamics and it does not depend on the interaction potential, which, in this report, we show that this is not true.

The exponent n in the equation 86 can be adapted depending the model. For example $n = 6$ will be use in this project. But it is used also with $n = 4$ for the interaction between an atom and an ion, $n = 6$ for neutral atoms and $n =$

7 for the Casimir-Polder potential between two neutral polarizable atoms. The potential is zero at $r = r_0$ and achieves its minimum $v_{min} = -u\frac{n-2}{2n-2}(\frac{n}{n-2})^{\frac{n}{n-2}}$ at $r_{min} = (\frac{2n-2}{n})^{\frac{1}{n-2}} r_0$. For more details of the process, to get the expression for the scattering length we can go to the reference [7]. The final expression will looks like ($x = r_0\sqrt{u}$):

$$a_{scatt} = r_0 \left(\frac{2x}{n-2} \right)^{\frac{1}{n-2}} \frac{\Gamma(\frac{-x+n-1}{2n-4})\Gamma(\frac{n-3}{n-2})}{\Gamma(\frac{-x+n-3}{2n-4})\Gamma(\frac{n-1}{n-2})} \tag{87}$$

For the case of $n = 6$, the behavior of the scattering length is shown in the figure 6

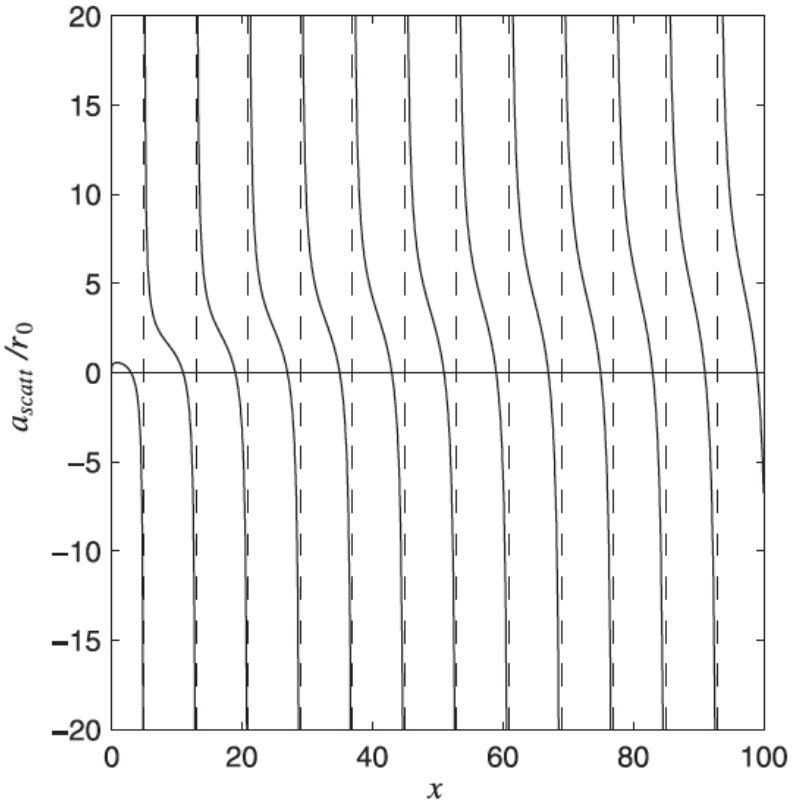

Figure 6: Scattering length a_{scatt}/r_0 in dependence of the variable $x = r_0\sqrt{u}$ for the case $n = 6$. The dashes lines mark the positions of the poles (from Ref. [7])

The properties of this expression are the following:

1. It is well-known that the constant cross section limit at zero energy is valid only for the potentials falling off faster than r^{-3}. The scattering length goes to infinity when $n \to 3+$.

2. Apart from the multiplicative factor r_0, the scattering length depends on two parameters only, namely n and x. In particular, this holds for the position of the poles and zeros. This fact allows for quite precise calculation in the case if scattering lengths are available for different isotopes.

3. Poles and zeros of the scattering length are given by the poles of $\Gamma(\frac{-x+n-1}{2n-4})$ and $\Gamma(\frac{-x+n-3}{2n-4})$, respectively. Poles of a_{scatt} occur at

$$x_{pole} = (2n-4)N_b + n - 1; \qquad N_b = 0, 1, 2, ...$$

   where N_b denotes the number of bound states; there are N_b bound states for $(2n-4)(N_b-1)+n-1 < x < 2n-4)N_b + n - 1$. Zeros at a_{scatt} occur at

$$x_{zero} = (2n-4)M + n - 3; \qquad N_b = 0, 1, 2, ...$$

4. The relative proportion of positive and negative values of a_{scatt} is given by $\frac{n-3}{n-2}$ and $\frac{1}{n-2}$. For $n = 6$, positive values occur three times more often than negative ones.

5. If x happens to lie in the neighborhood of a pole, any minor uncertainty in the shape of the potential can easily provoke big changes in the scattering length. On the other hand, this means that in this situation, the potential parameters may be fixed very precisely even if the scattering length is known with a modest degree of accuracy.

4.2 Binding energy as a function of the strength interaction for the Bipolaron problem

As an introduction to the model and the code that calculate the energies in the ground states using the (HNC-EL) theory, initially I reproduced the behavior of the bound energy as a function of the wave number of the bipolaron [1] for two bosonic impurities with $m = m_B$. In the Fig 7 the results of Camacho-Guardian et al. are shown [8]. In the part (a) of this plot, there is a cartoon that illustrate the Bose polarons forming a bipolaron as a consequence of the phonon mediated interaction. In (b) the binding energy is represented as a function of the impurity boson interaction strength for two bosonic impurities with $m = m_B$. The red solid

[1] Bipolarons are two quasiparticles, the so-called polarons that form a bound state much smaller than the average distance between the unbound polarons.

belongs to the case when $n_B a_B^3 = 10^{-6}$ ($n_B = \rho = 0.0001$) and $n_B a_B^3 = 10^{-5}$ ($\rho = 0.001$). (c) It shows the corresponding inverse size $\sigma^{-1} = \xi_B \sqrt{\langle r^2 \rangle}$ of the bipolaron wave function.The arrows indicate the critical values of strength to form a bound state.

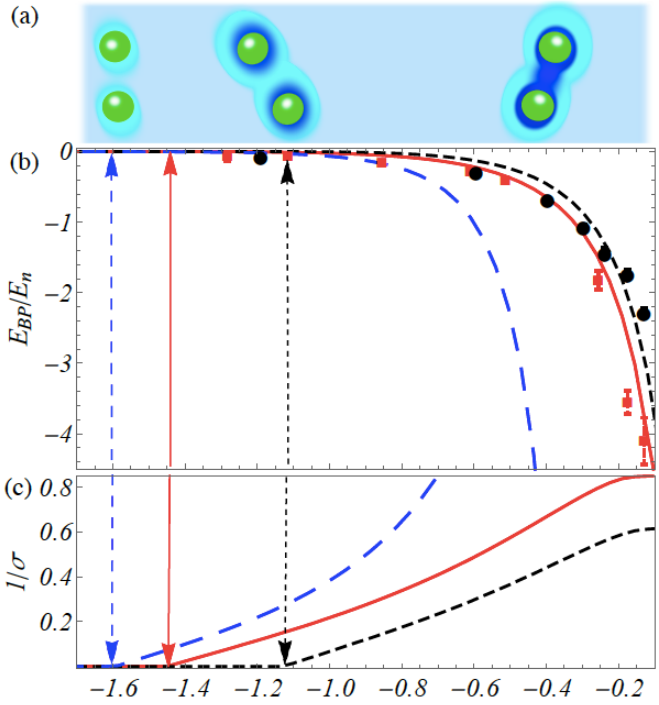

Figure 7: (a) Creation of bipolarons due to the mediated interaction. (b) Binding energy E_{BP} of the bipolaron as a function of the interaction strength. (c) σ^{-1} of the bipolaron wave function. (from [8])

Using the code and the same values we reproduced these results for the case of $\rho = 0.001$ (black points), $\rho = 0.0001$ (red points) and $\rho = 0.0002$ (green points) as is shown in the figure 8, which indicates good qualitative agreement with the results of the paper [8], because we will show that the behavior of the binding energy depend on more than just the scattering length .

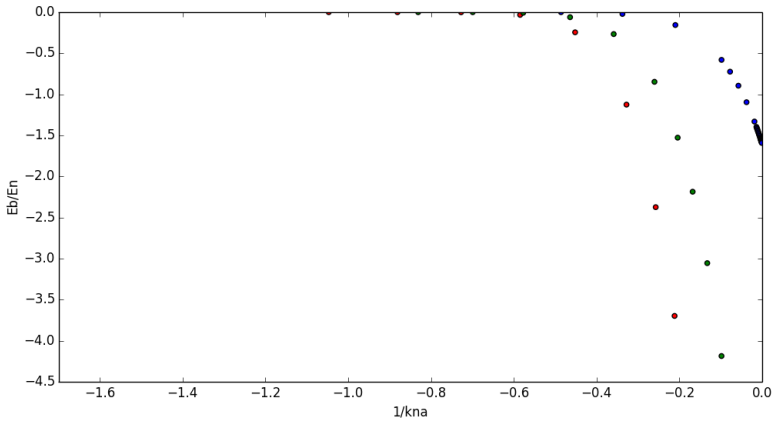

Figure 8: Binding energy against the scattering length $(1/k_n a)$. Black points correspond to $\rho = 0.001$, red points are for the density $\rho = 0.0001$ and green points represent $\rho = 0.0002$

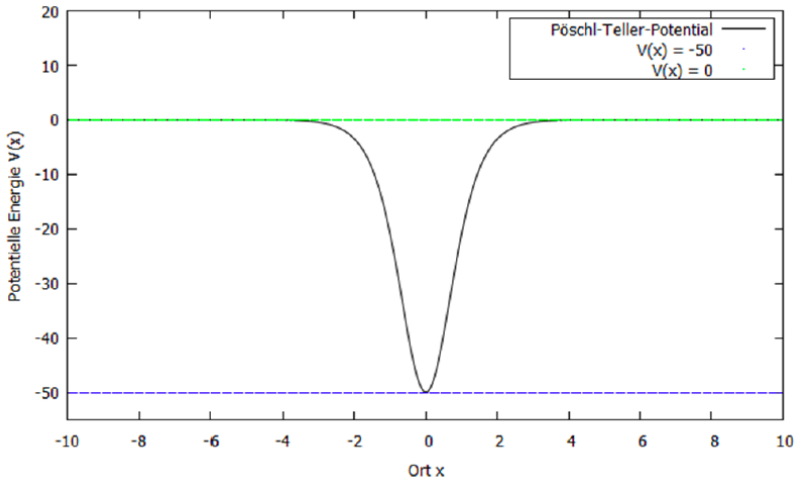

Figure 9: Pöschl-Teller Potential example for $\rho = 1$ and $V_0 = 50$

4.3 Pöeschl-Teller Potential

The Pöschl-Teller Potential described in the equation 88, -named after the two physicists Herta Pöeschl and Edward Teller- represents a short-range, attractive well potential, which in particular for the description of systems for diatomic molecules. In figure 9, we present the plot for some values of the constant $\rho = 1$ and $V_0 = 50$ as an example.

$$V(x) = -\frac{V_0}{\cosh^2(x/\rho)}, \tag{88}$$

With the definitions of $\cosh(x)$:

$$\cosh(x) = \frac{1}{2}(e^x + e^{-x}), \tag{89}$$

studying the limit behavior of Pöschl-Teller Potential we get:

$$\lim_{x\to\pm\infty}\left(-\frac{V_0}{\cosh^2(x/\rho)}\right) = \lim_{x\to\pm\infty}\left(-\frac{4V_0}{e^{2x}+e^{-2x}+2}\right) = 0 \tag{90}$$

also,

$$\lim_{x\to 0}\left(-\frac{V_0}{\cosh^2(x/\rho)}\right) = -\frac{V_0}{\cosh^2(0)} = -V_0 \tag{91}$$

Then now,

$$-\cosh^2(x/\rho) = -(1/4)(e^{x/\rho} + e^{-x/\rho})^2 \tag{92}$$

at the position $x = 0$ there is a global maximum, the Pöschl-Teller Potential also has a minimum. The parameter V_0 of the Pöschl-Teller Potential reflects the depth of the potential well at the position $x = 0$. The minimum goes to zero as well as the limit to infinity showed in the equation 90. The parameter ρ characterize the range of the potential. Specially small values of ρ reflect short range interactions, as it is summarize in the Figure 10. Taken from [9].

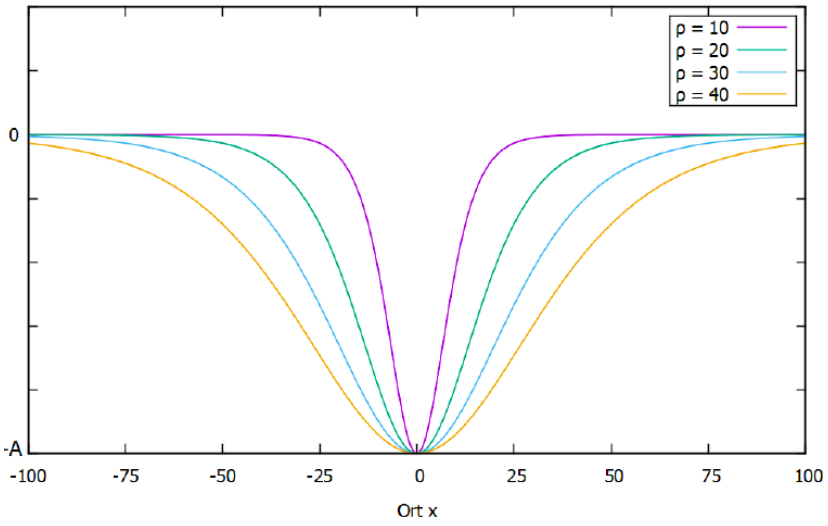

Figure 10: Pöschl-Teller Potential example for different values of ρ and $V_0 = 50$

4.3.1 Scattering Length for the Pöschl-Teller Potential

The analytical expression for getting the scattering length using the Pöschl-Teller Potential is given by:

$$a_{scatt} = r_c\left(\frac{-1}{V_0} + \frac{\pi}{2\tan(\pi V_0/2)} + \gamma + pg\right) \tag{93}$$

where γ is the euler‘s constant and is equal to

$$\gamma = 0.57721566490153286060651209008240243104 2...$$

and pg is given by

	X=r*sqrt(u) <5	a=-1	a=-4	a=-10	a=-14	a=-16	a=-25	a=-50	a=-100	a=-300
V0	r_max	r	r	r	r	r	r	r	r	r
2	3.535533906		2.83394	3.1083	3.19453	3.22557				
4	2.5	1.78834	2.08018	2.26058	2.31302	2.3314	2.38295	2.43659	2.46688	2.48862
6	2.041241452		1.73396	1.87241	1.91091	1.9242				
8	1.767766953		1.5228	1.63657	1.66726	1.67776	1.70649	1.73525	1.75099	1.76205
10	1.58113883	1.1878								
12	1.443375673									
14	1.33630621	1.02283	1.1806	1.25675	1.27617		1.30028	1.31744	1.32664	1.33303
16	1.25									
18	1.178511302									
20	1.118033989	0.873023	1.00234	1.06054	1.0749	1.07968				
22	1.066003582	0.836845	0.959253	1.01333	1.02656	1.03095	1.04265	1.05388	1.05982	1.06392
23	1.04257207	0.820486	0.939767	0.992009	1.00474	1.00897				
24	1.020620726	0.805122	0.921466	0.972003	0.984274	0.988343	0.999149	1.00949	1.01495	1.01871
25	1		0.904231	0.95318	0.965024	0.968947				

Table 1: Values a and r_c using Lennard-Jones potential. Here different combinations of V and r were calculated for getting the same scattering length a.

$$pg = \frac{d \log \Gamma(V_0 + 1)}{dV_0}$$

4.4 Single impurity

Use Lennard-Jones 10-6 and Pöschl-Teller Potential as implemented in vbare.f90; they are both characterized by a strength parameter V_0 and width parameter r_c, to be set in the command file. Let the background density be $\rho = 10^{-3}$, 10^{-4}, 10^{-5} and 10^{-6}.

4.4.1 Negative scattering length a

We choose different V_0 and r_c in the two potentials such that a is the same and compare $g_I(r)$ and $S_I(k)$ for a between -0.5 and $-\infty$. How negative can you go with a until $g_I(r)$ and $S_I(k)$ depend not just on a (i.e. non-universal behavior.)?

First, we used the Lennard Jones potential. For negative values of scattering lengths (scattering states) and using the equation 87 with $n = 6$, we get the different combinations of V_0 (or u) and r_c (or σ) such a way that we get the same scattering length. As an example, I used the combinations shown in Table 1.

The second column show the maximum value that x and r can take depending on the divergences in the behavior of the scattering lengths. The idea again, is not go into bound states or divergences, just scattering states. $g(r)$ and $S(k)$ will be calculated for several values of the scattering lengths as is shown:

In the Figure 11 I present the behavior of $S(k)$ and $g(r)$, except in Figure 11(a)

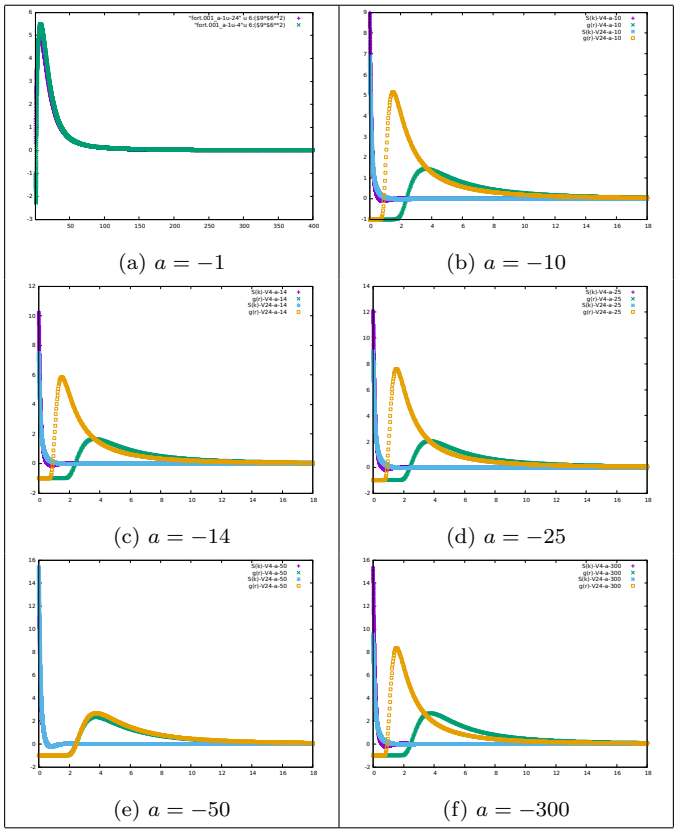

(a) $a = -1$ (b) $a = -10$

(c) $a = -14$ (d) $a = -25$

(e) $a = -50$ (f) $a = -300$

Figure 11: Plots of $g(r)$ and $S(k)$ for $\rho = 0.001$ using two values of V_0: 4 and 24 in the Lennard-Jones potential. The green plot of $g(r)$ corresponds to $V_0 = 4$ and the yellow $g(r)$ corresponds to the combinations using $V_0 = 24$.

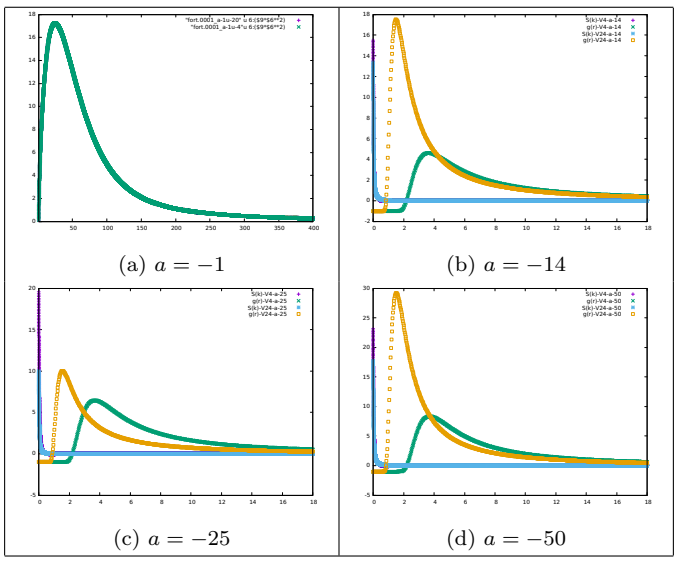

(a) $a = -1$ (b) $a = -14$

(c) $a = -25$ (d) $a = -50$

Figure 12: Plots of $g(r)$ and $S(k)$ for $\rho = 0.0001$ using two values of V_0: 4 and 24 in the Lennard-Jones potential, except in the part (a) where $r^2 g(r)$ is shown for $V_0 = 20$ and $V_0 = 4$. The green plot of $g(r)$ corresponds to $V_0 = 4$ and the yellow $g(r)$ corresponds to the combinations using $V_0 = 24$.

where $r^2 g(r)$ is shown. Here we used the Lennard-Jones potential in a density of $\rho = 0.001$ and $V_0 = 4$ and $V_0 = 24$ which gave me a difference of the values of $r_c \approx 1.3$ (better shown in Table 1) for all the scattering lengths. We can observe that for all the scattering length there is a remarkable difference in the correlation function $g(r)$ for values in the range of $r <\approx 5$. Except for $a = -50$ and $a = -1$.

For results in the Figure 12, I used four of the same scattering length but in this case I am using a smaller density $\rho = 0.0001$. We can observe a similar behavior but for smaller scattering lengths, the differences between $g(r)$ are more remarkable for larger range of r.

For results with smaller density $\rho = 0.00001$ in Figure 13, we can observe that a larger maximum is getting when we use a larger strength of V_0 and while we decrease the value of the scattering length. Also I could say that the difference between the correlation functions can start around $r > 6$ in general, and that while the density gets smaller values, the system is not affecting the interaction between the impurity and the particle of the system.

Figure 14 show results for smallest density $\rho = 0.000001$. We see the same behavior but in this case the maximum is more remarkable if we compare between same scattering length plots but different densities. The system is not affecting

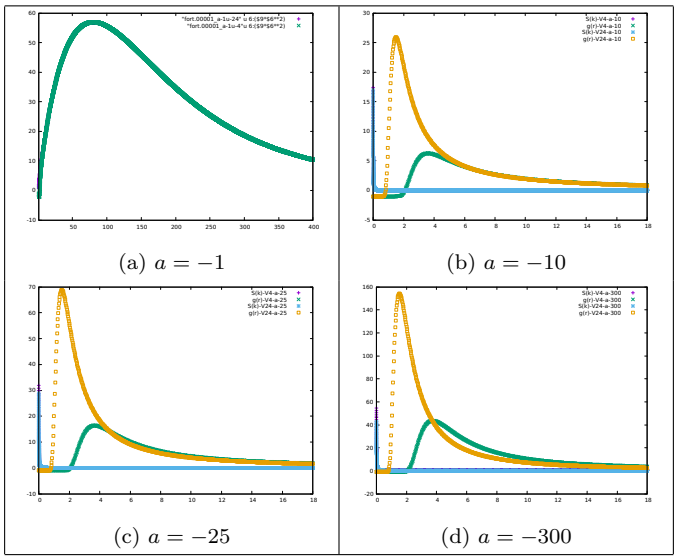

(a) $a = -1$ (b) $a = -10$

(c) $a = -25$ (d) $a = -300$

Figure 13: Plots of $g(r)$ and $S(k)$ for $\rho = 0.00001$ using two values of V_0: 4 and 24 in the Lennard-Jones potential, except in the part (a) where $r^2 g(r)$. The green plot of $g(r)$ corresponds to $V_0 = 4$ and the yellow $g(r)$ corresponds to the combinations using $V_0 = 24$.

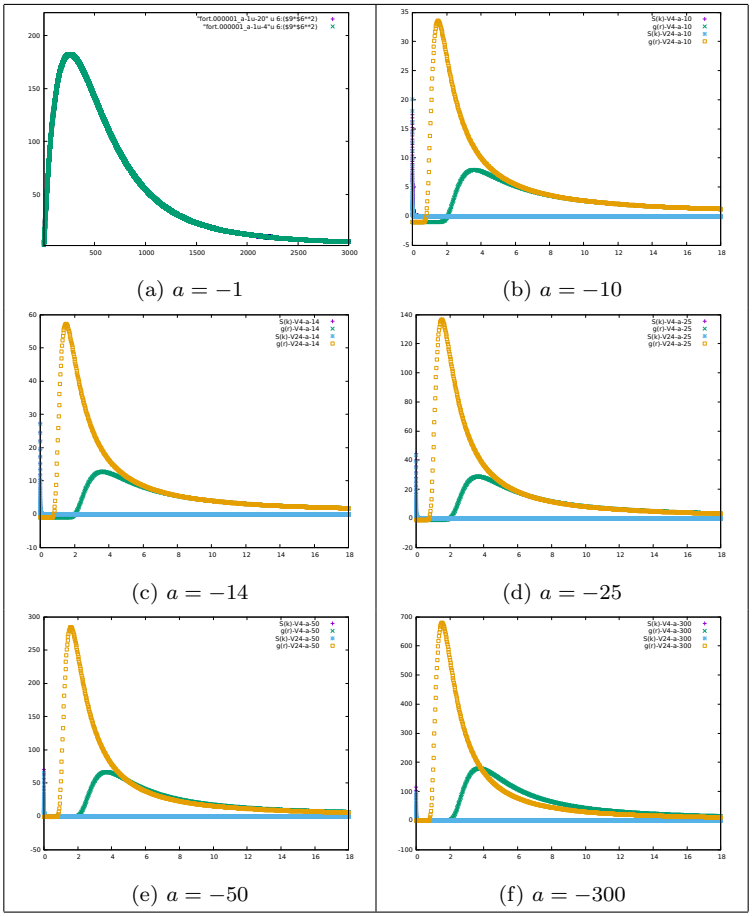

(a) $a = -1$ (b) $a = -10$

(c) $a = -14$ (d) $a = -25$

(e) $a = -50$ (f) $a = -300$

Figure 14: Plots of $g(r)$ and $S(k)$ for $\rho = 0.000001$ using two values of V_0: 4 and 24 in the Lennard-Jones potential, except in the part (a) where $r^2 g(r)$ and $V_0 = 4$ and $V_0 = 20$. The green plot of $g(r)$ corresponds to $V_0 = 4$ and the yellow $g(r)$ corresponds to the combinations using $V_0 = 24$.

	a=-1	a=-4	a=-10	a=-50
r	v0	v0	v0	v0
0.2	1.834	1.9524	5.98088	1.99602
0.4	1.71712	1.90921	1.44803	1.99206
0.5	1.67084	1.78369	1.9524	1.9901
0.9	1.53571	1.8172	1.91752	7.98281
1	1.5105	1.8011	3.91581	5.98088
1.5	1.41465	1.72978	1.8699	1.97088
1.3	1.44803	1.75662	1.88519	1.97466
1.8	1.37335	1.69315	1.84798	3.96625
1.9	1.36144	1.6818	1.84093	7.96544
1.99	1.35138	1.67192	1.83469	1.96173

Table 2: Values of r_c and V using the Pöschl-Teller Potential

the behavior of the impurity and the results show a two-particle behavior.

Now, using the Pöschl-Teller Potential, and getting the combinations of V_0 and r_c using the equation 93 we get the following results (We observe that the value of V_0 can be just between 0 and 2, before getting the divergence that will guide us to bound states):

Using the Pöschl-Teller Potential, this time we only plotted $r^2 * g(r)$. As we can see for the density $\rho = 0.001$ in Figure 15 there are some differences between the plots that are calculated for the same scattering length. Also, it is important to see that $g(r)$ has different behavior using the same scattering length, which it is displayed in the plots (c) and (d) that, for the same scattering length (-39), the behavior of $g(r)$ differs for two combinations of V_0 and r_c. For smaller density $\rho = 0.0001$ in Figure 16, we get a similar behavior, but the peaks take larger values as we observed for the Lennard-Jones Potential.

4.4.2 Positive scattering length a

Using the mathematical expression 87 for getting the values of V_0 and r_c for positive a, in the Table 3 are shown the combinations of V_0 and r_c in order to testing the behavior of $g(r)$ with the scattering length.

The results for a positive, using the Lennard-Jones potential, display a similar behavior when the $g(r)$ does not depend only of the scattering length, also depend of V_0 and r_c. We observe an increasing peak in the function $g(r)$ when the density is small but the physical character of having a positive scattering length, which could allow bound states, do the comparison and the generalization a little difficult.

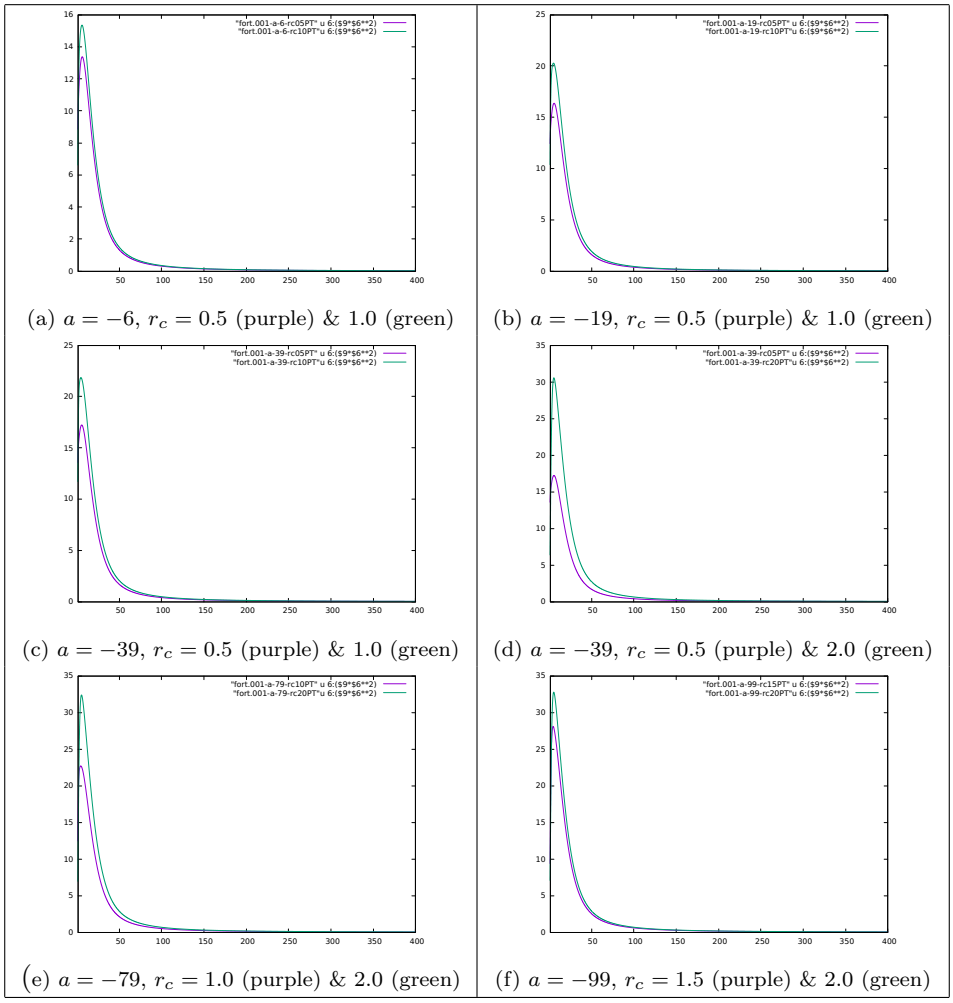

(a) $a = -6$, $r_c = 0.5$ (purple) & 1.0 (green)

(b) $a = -19$, $r_c = 0.5$ (purple) & 1.0 (green)

(c) $a = -39$, $r_c = 0.5$ (purple) & 1.0 (green)

(d) $a = -39$, $r_c = 0.5$ (purple) & 2.0 (green)

(e) $a = -79$, $r_c = 1.0$ (purple) & 2.0 (green)

(f) $a = -99$, $r_c = 1.5$ (purple) & 2.0 (green)

Figure 15: Plots of $r^2 g(r)$ for $\rho = 0.001$ using the Pöschl-Teller Potential.

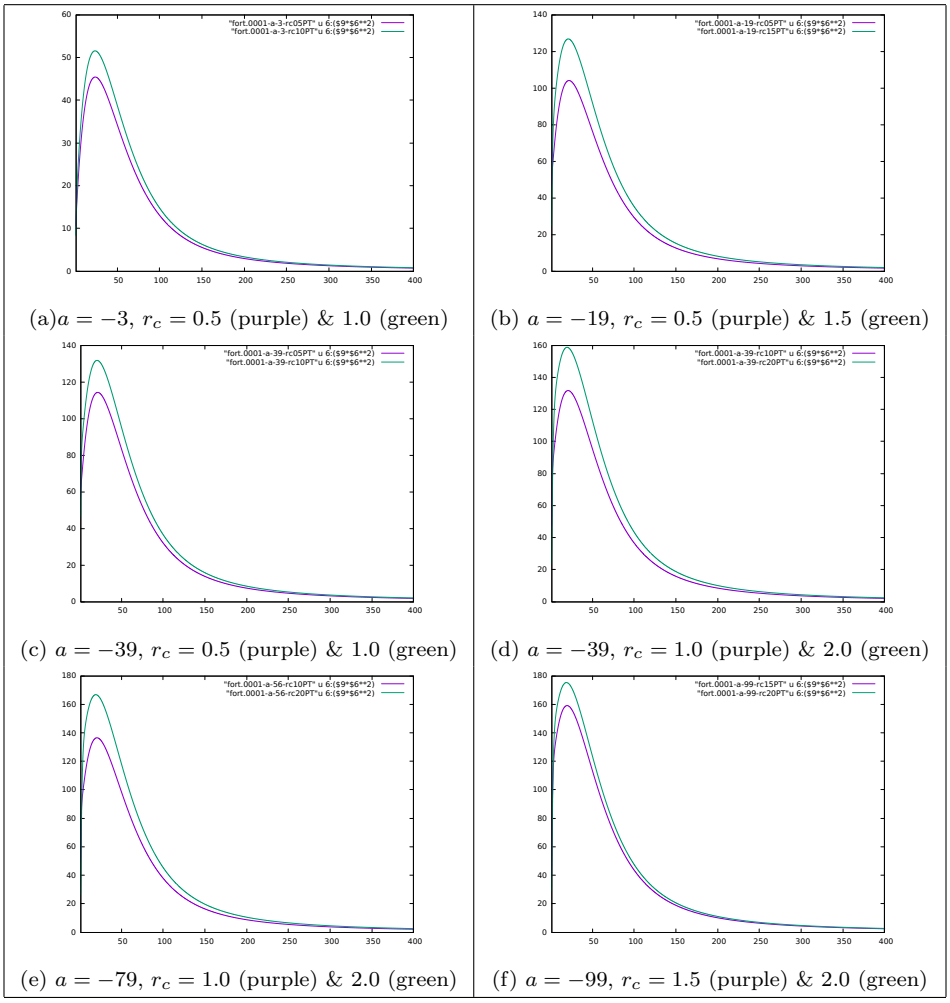

(a)$a = -3$, $r_c = 0.5$ (purple) & 1.0 (green)

(b) $a = -19$, $r_c = 0.5$ (purple) & 1.5 (green)

(c) $a = -39$, $r_c = 0.5$ (purple) & 1.0 (green)

(d) $a = -39$, $r_c = 1.0$ (purple) & 2.0 (green)

(e) $a = -79$, $r_c = 1.0$ (purple) & 2.0 (green)

(f) $a = -99$, $r_c = 1.5$ (purple) & 2.0 (green)

Figure 16: Plots of $r^2 g(r)$ for $\rho = 0.0001$ using the Pöschl-Teller Potential.

u	a=1	a=4	a=10	a=14	a=25	a=50	a=300
2					3.92359		
4	5.42126	5.07532	3.25196	2.8915	2.6729	2.5768	2.51175
5	4.83982		2.76276	2.52966	2.37075	2.29681	2.24545
6	4.41047		2.44435	2.27533	2.15136	2.09144	2.04905
7	4.07667				1.98285	1.93258	1.89651
8	3.8075		2.04006	1.93349	1.84824	1.80498	1.77361
10	3.3957	2.88198	1.78558	1.70892	1.64442	1.61068	1.58581
12	0.0915				1.49546		1.44726
14	2.85487				1.38053		1.33964
16	2.66398	1.93401	1.36559	1.32513	1.2884	1.26822	3.26222
17	2.58137					1.2298	3.16446
18	2.50572				1.21243	1.19466	3.07498
20	2.37172	1.56594			1.14841	1.13253	2.91664
22	2.25632	1.44178	1.14596	1.11893	1.09349	1.07915	2.78047
23	2.20432	1.38976					1.0446
24	2.15557	1.34304	1.09305	1.06877	1.04572	1.03265	2.66173

Table 3: Values of the combinations of V_0 and r_c using the Lennard-Jones Potential, for getting the $a`s$ (positive)

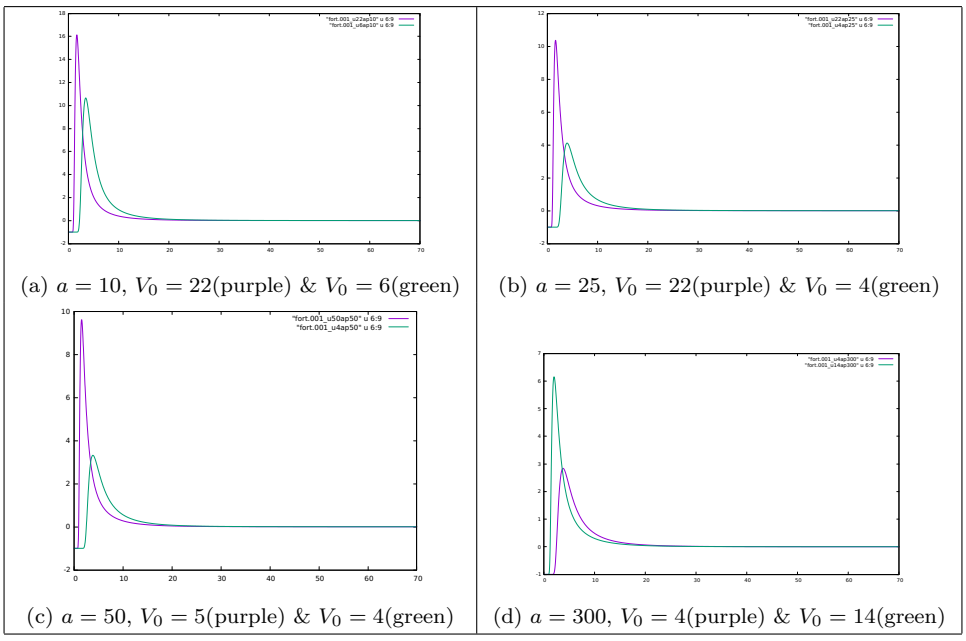

(a) $a = 10$, $V_0 = 22$(purple) & $V_0 = 6$(green)

(b) $a = 25$, $V_0 = 22$(purple) & $V_0 = 4$(green)

(c) $a = 50$, $V_0 = 5$(purple) & $V_0 = 4$(green)

(d) $a = 300$, $V_0 = 4$(purple) & $V_0 = 14$(green)

Figure 17: Values using positive scattering length and the Lennard-Jones potential for $\rho = 0.001$

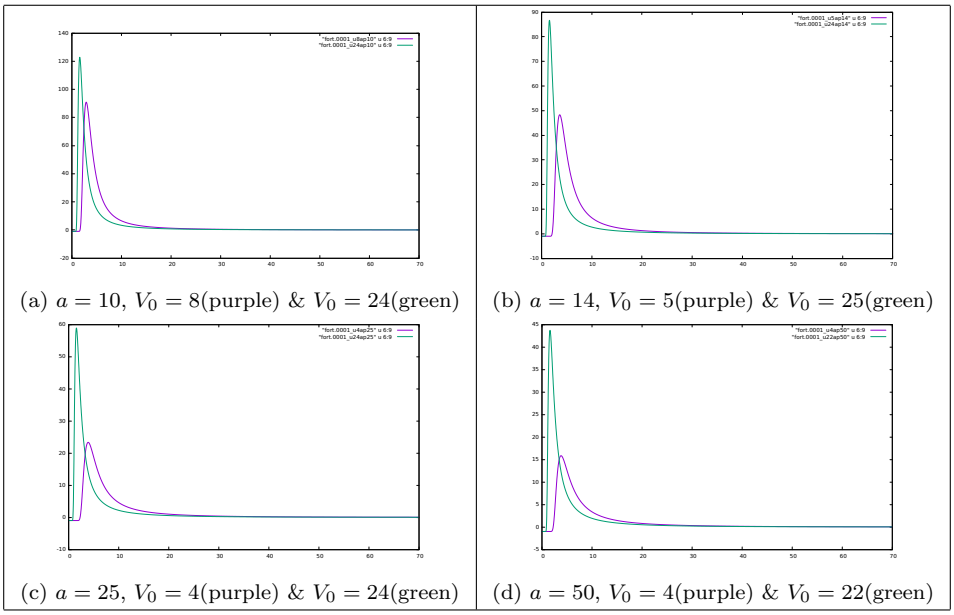

(a) $a = 10$, $V_0 = 8$(purple) & $V_0 = 24$(green)

(b) $a = 14$, $V_0 = 5$(purple) & $V_0 = 25$(green)

(c) $a = 25$, $V_0 = 4$(purple) & $V_0 = 24$(green)

(d) $a = 50$, $V_0 = 4$(purple) & $V_0 = 22$(green)

Figure 18: Values using positive scattering length and the Lennard-Jones potential for $\rho = 0.0001$

5 Triplet Correlations

We use the Pöschl-Teller Potential with a given choice of r_c and compare the results for chemical potential, $g_I(r)$ and $S_I(k)$ with and without triplet correlations for the same three densities; start again with $a = -0.5$ and decrease a towards $-\infty$ as long as possible. Caution: the HNC-EL iterations may not converge as you go to larger $|a|$.

I got triple correlations just for small density and $a = -4$. Probably this part requires more testing.

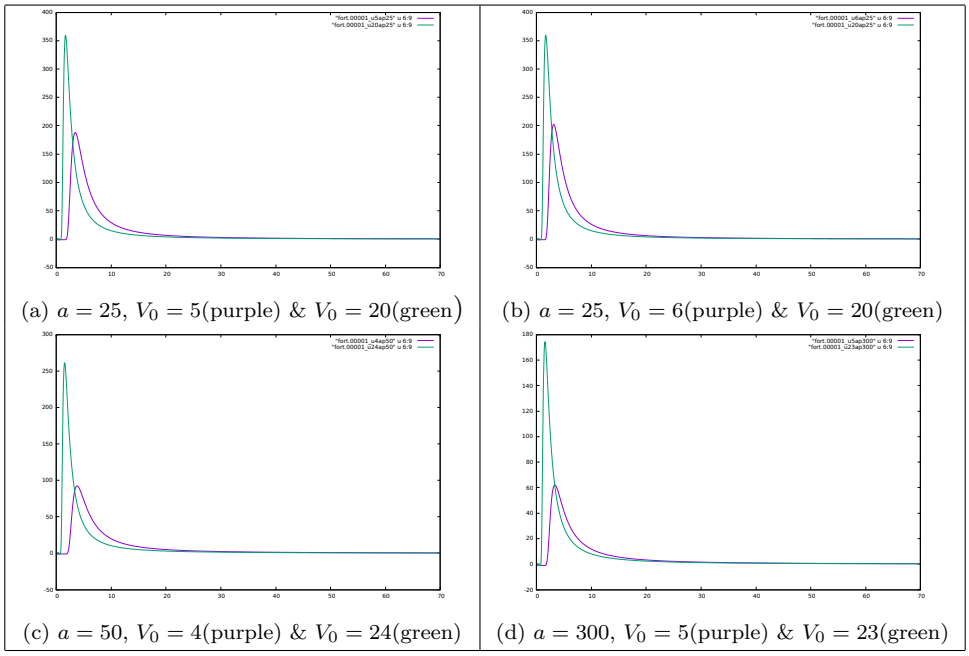

(a) $a = 25$, $V_0 = 5$(purple) & $V_0 = 20$(green)

(b) $a = 25$, $V_0 = 6$(purple) & $V_0 = 20$(green)

(c) $a = 50$, $V_0 = 4$(purple) & $V_0 = 24$(green)

(d) $a = 300$, $V_0 = 5$(purple) & $V_0 = 23$(green)

Figure 19: Values using positive scattering length and the Lennard-Jones potential for $\rho = 0.00001$.

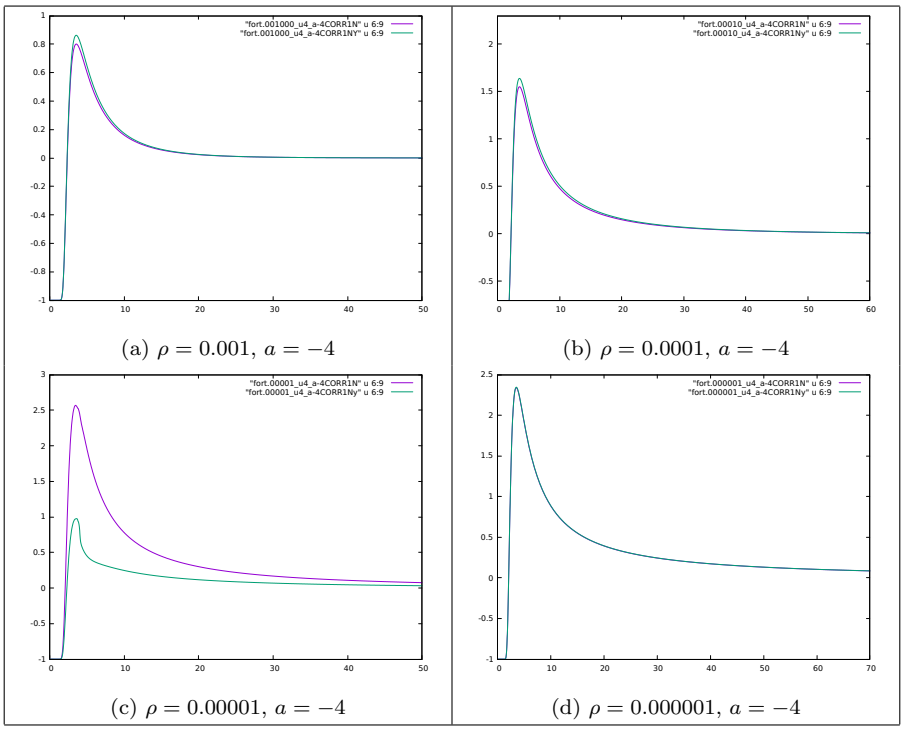

(a) $\rho = 0.001$, $a = -4$

(b) $\rho = 0.0001$, $a = -4$

(c) $\rho = 0.00001$, $a = -4$

(d) $\rho = 0.000001$, $a = -4$

Figure 20: Correlations of $a = -4$ and for different densities using Lennard-Jones potential. Green plots consider correlations while the purple shows results without correlations, all for the value $V_0 = 4$.

6 Conclusions

1. As expected, for a negative scattering length, the correlation function $g(r)$ shows a peak that increases with increasing $|-a|$, which means that the probability of dispersion between the impurity and the particle is larger. This was observed for both types of potential , the Lennard- Jones Potential and Pöschl-Teller Potential.

2. The results for $S(k)$ and $g(r)$ corresponding to low densities obey the behavior of two interacting particles. This can be seen, for example, in the plots for the Lennard-Jones potential in $a = -25$: the density ρ goes from 0.001 to 0.000001 and the peaks of $g(r)$ take approximately the values 8, 10, 70 and 140 respectively. This was observed for the two potentials.

3. Using the Lennard-Jones potential, we were able to study the behavior of $g(r)$ for positive and negative scattering lengths. The peaks for negative scattering lengths increase with the increasing of $|-a|$; in the another hand, the peaks of $g(r)$ decrease using positive increasing scattering length a, which also correspond to the situation of get away from a bound state as was illustrated in the Figure 3.

4. It would be possible to establish a range from where only depends on scattering length. This is because from the results, the values in the $g(r)$ function has not a remarkable difference after some point. For example, using the Lennard-Jones Potential, $g(r)$ start being independent close to $r = 18$, except for the case when the density is $\rho = 0.001$, the function shows an independence close to $r = 8$. For positive a, $g(r)$ shows an independence around the value $r = 20$. Considering the Pöschl-Teller Potential although I plotted $r^2 g(r)$, this function shows an independence after $r \approx 150$.

5. There is not a relevant response in the inclusion of triplet correlations for the system with one impurity using the code, the results that I got only corresponds to small scattering length a. This part probably needs more exploration.

References

[1] A. Atland. *Notes of Class in Advanced Quantum Mechanics*, 2007.

[2] G. Mahan. *Many-Particle Physics*. 2000.

[3] D. Hufnagl. Strongly correlated dipolar bose gases. *Dissertation of doctoral thesis.*, 2013.

[4] M. Saarela and E. Krotscheck. *Journal of Low Temp. Phys.*, 90:415, 1993.

[5] Eugene Feenberg. *Theory of Quantum Fluids*. 1969.

[6] J. C. Owen. *Phys. Rev. Lett.*, 47:586, 1981.

[7] J. Pade. *Eur. Phys. J. D.*, 44:345–350, 2007.

[8] A. Camacho-Guardian, L. A. Peña Ardila, T. Pohl, and G. M. Bruun. *Phys. Rev. Lett.*, 121:013401, 2018.

[9] Okan Askar. TWKB approximation and exact solution of the Pöschl-Teller potential. https://www.uni-muenster.de/imperia/md/content/physik_tp/theses/muenster/askar-ba.pdf, 2010 (accessed September 24, 2018).

[10] R. P. Feynman. *Phys. Rev*, 94:262, 1954.

[11] J. Tempere, W. Casteels, M. K. Oberthaler, S. Knoop, E. Timmermans, and J. T. Devreese. *Phys. Rev. B*, 80:184504, 2009.